Electronic Supplementary Material (ESI) for Nanoscale.
This journal is © The Royal Society of Chemistry 2020

Visible to Near-Infrared Photodetector with Novel Optoelectronic Performance Based on Graphene/S-doped InSe Heterostructure on h-BN Substrate

Qiaoyan Hao,[a] Jidong Liu,[a] Weilong Dong,[a] Huan Yi,[a] Yuxuan Ke,[a] Sisi Tang,[a] Dianyu Qi,[a] Wenjing Zhang*,[a]

Step 1, h-BN was mechanically exfoliated onto SiO_2/Si substrate. The picture above shows the bright field (BF) image of the h-BN flake. To increase the contrast, the dark filed (DF) image was also acquired. Step 2, $InSe_{0.9}S_{0.1}$ was exfoliated on a transparent polydimethylsiloxane (PDMS) stamp. We note that the surface of the $InSe_{0.9}S_{0.1}$ flake was very clean without obvious bump or bubbles. Step 3, the $InSe_{0.9}S_{0.1}$ flake on PDMS was aligned on the target h-BN flake using the home-made micromanipulator. After that, some islands were observed at the $InSe_{0.9}S_{0.1}$/h-BN interface, which should be associated with the trapped air bubbles that formed during the transfer process. Step 4-5, graphene was exfoliated on a PDMS stamp and located to cover the target $InSe_{0.9}S_{0.1}$ flake to prepare the heterostructure finally. Some islands were also observed at the graphene/$InSe_{0.9}S_{0.1}$ or graphene/h-BN interfaces.

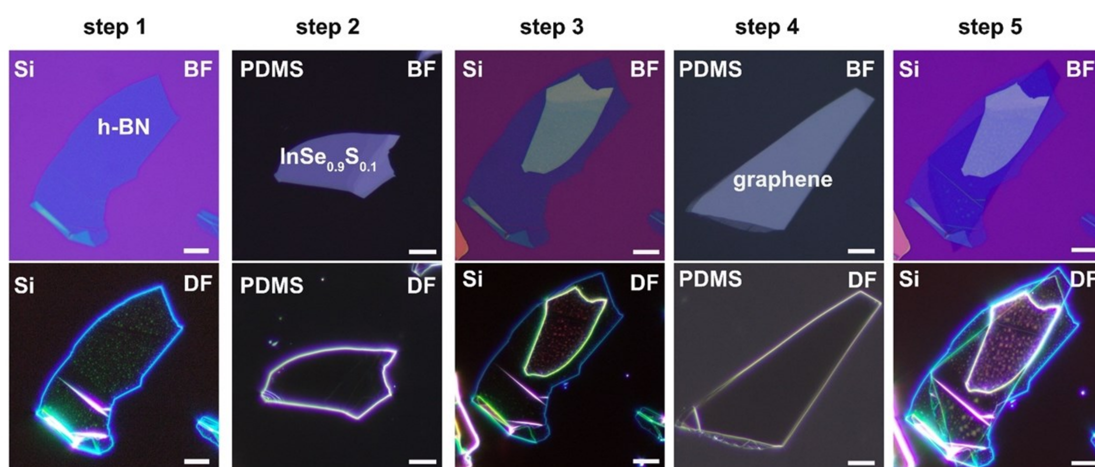

Figure S1. Dry transfer process to fabricate a graphene/$InSe_{0.9}S_{0.1}$ heterostructure on h-BN. Scale bars, 10 µm.

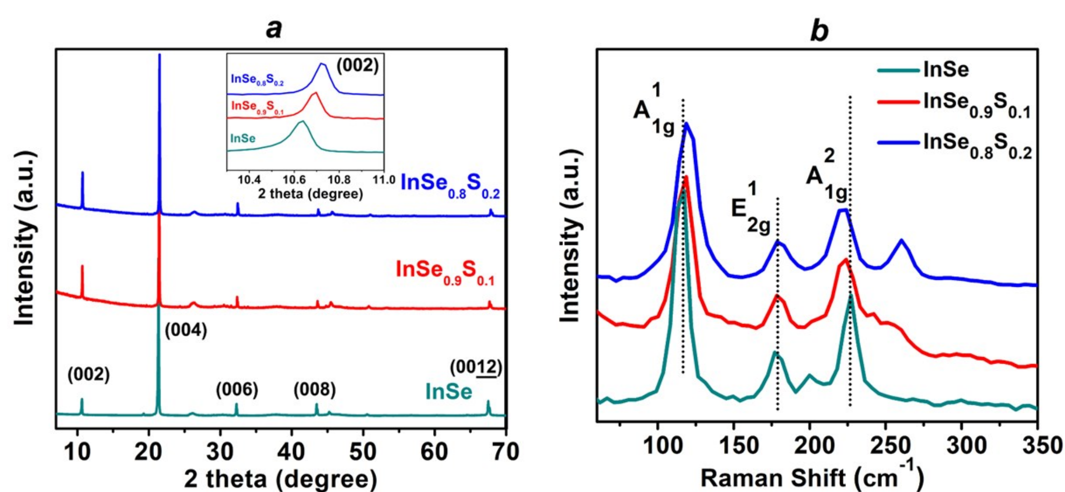

Figure S2. (a) XRD patterns of pure InSe and its S-doped alloys, insert shows the zoom-in view of the (002) diffraction peaks. (b) Raman spectra of pure InSe and its S-doped alloys. It was found that, as the S ratio increased, the A1 1g mode showed a blue-shift trend, while the A2 1g mode showed a red-shift trend. In contrast, the E1 2g mode remained at nearly the same frequency as the S ratio increased.

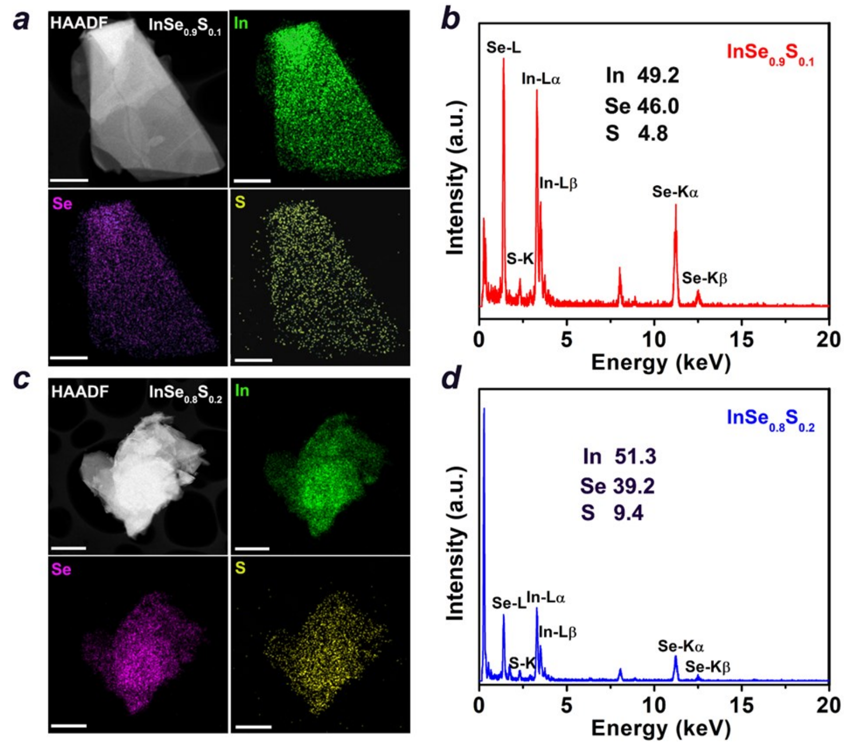

Figure S3. (a) High angle annular dark-field (HAADF) image and corresponding EDS elemental mapping of $InSe_{0.9}S_{0.1}$ flake. Scale bars, 1 µm. (b) EDS spectrum obtained from $InSe_{0.9}S_{0.1}$ flake. (c) HAADF image and corresponding EDS elemental mapping of $InSe_{0.8}S_{0.2}$ flake. Scale bars, 2 µm. (d) EDS spectrum obtained from $InSe_{0.8}S_{0.2}$ flake. The actual compositions of $InSe_{0.9}S_{0.1}$ and $InSe_{0.8}S_{0.2}$ were determined to be $InSe_{0.93}S_{0.10}$ and $InSe_{0.76}S_{0.18}$, respectively, close to their nominal compositions within the error of the measurements.

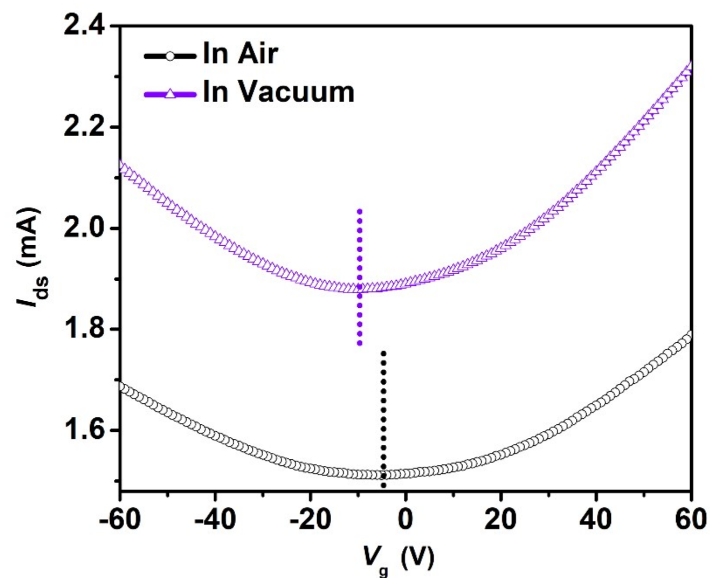

Figure S4. Transfer curves (I_{ds}-V_g) of the device based on graphene/h-BN in the dark under ambient conditions and

in vacuum (V_{ds} = 1 V).

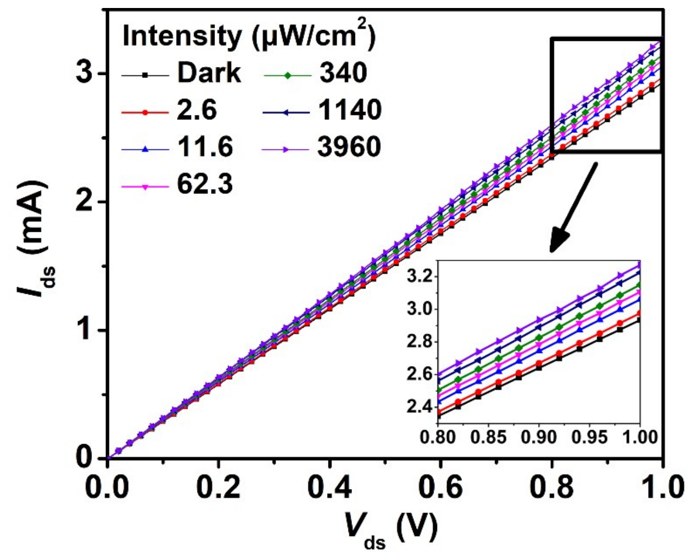

Figure S5. Output characteristics (I_{ds}-V_{ds}) of the device based on graphene/$InSe_{0.9}S_{0.1}$ heterostructure in the dark and under illumination with various excitation intensities (V_g = 0 V, λ = 700 nm).

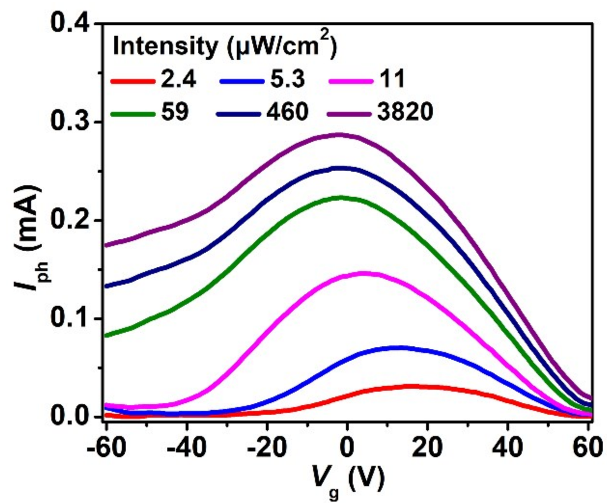

Figure S6. Gate voltage-dependent photocurrent (I_{ph}-V_g) of the graphene/$InSe_{0.8}S_{0.2}$ heterostructure device under different light power densities.

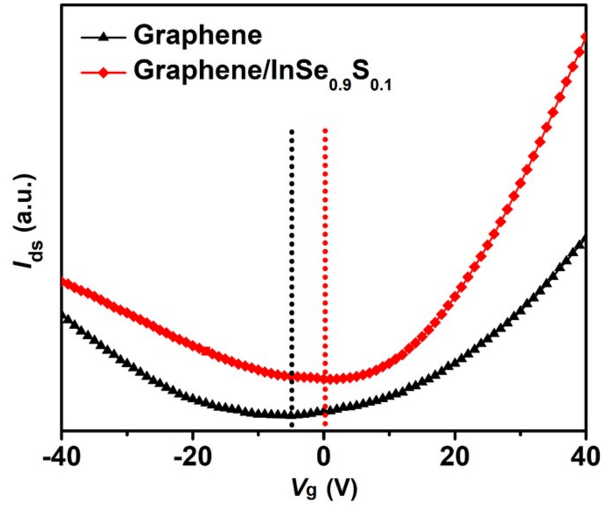

Figure S7. Transfer curves (I_{ds}-V_g) of the devices based on pure graphene and graphene/$InSe_{0.9}S_{0.1}$ heterostructure in the dark under ambient conditions (V_{ds} = 1 V).

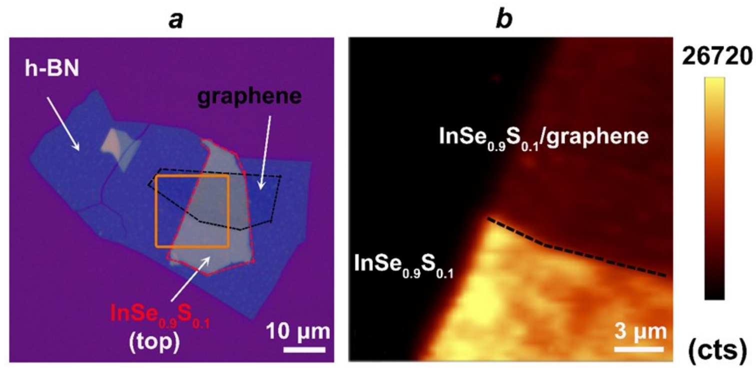

Figure S8. (a) Optical image of an $InSe_{0.9}S_{0.1}$/graphene heterostructure on h-BN. (b) PL mapping at about 1.29 eV ($InSe_{0.9}S_{0.1}$) of the area marked with the square in (a).

We investigated the optoelectronic performance of the $InSe_{0.9}S_{0.1}$-based devices. Figure S9a shows the output characteristics (I_{ds}–V_{ds}) of the $InSe_{0.9}S_{0.1}$-based device at different gate voltages. The current increased with increasing positive gate voltage, which is a clear signature of the *n*-type semiconductor behavior. The on/off current ratio exceeded 10^8 according to the transfer characteristics (I_{ds}–V_g) in Figure S9b. Figure S9c presents the photocurrent as a function of illumination intensity at V_g = 0 V and 50 V, respectively. A maximum photoresponsivity of 1.6×10^4 A/W was achieved at a low light power density of 7.0 μW/cm^2 and V_g = 50 V for the $InSe_{0.9}S_{0.1}$ photodetector as shown in Figure S9d, which was two orders of magnitude smaller than that (4.9×10^6 A/W) of graphene/$InSe_{0.9}S_{0.1}$ heterostructure device.

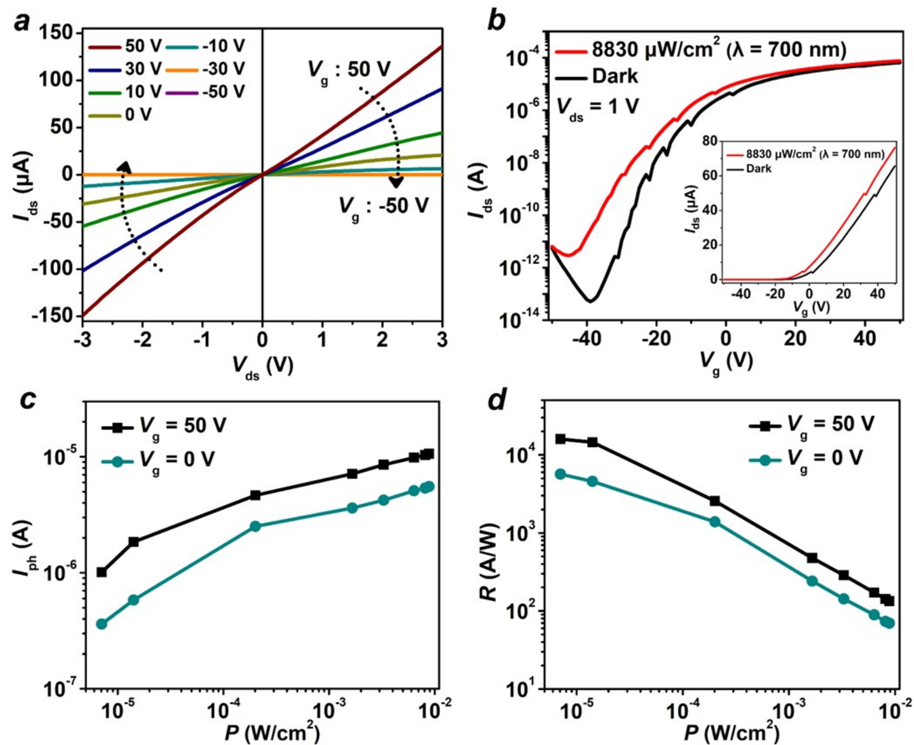

Figure S9. (a) Output curves of the $InSe_{0.9}S_{0.1}$-based device at different gate voltages. (b) Transfer curves of the $InSe_{0.9}S_{0.1}$-based device in the dark and under a light power density P = 8830 μW/cm^2 (V_{ds} = 1 V, λ = 700 nm) on logarithmic and linear (insert) scales. Measured photocurrent (c) and photoresponsivity (d) as a function of illumination intensity (V_{ds} = 1 V, λ = 700 nm) for the $InSe_{0.9}S_{0.1}$-based device.

Table S1. Comparison of device performance for Graphene/2D semiconductor photodetectors.

Materials	Spectral range	R [A/W]	*EQE/Gain*	Response time (ms)	Ref.
Graphene/S-doped InSe	Visible-NIR	4.9×10^6	*EQE* 8.7×10^8%	41	This work
Graphene/BP	Visible-NIR	1.3×10^3	*Gain* 1.13×10^9	4	1
Graphene/$MoTe_2$	Visible-NIR	970	*Gain* 4.69×10^8	78	2
Graphene/InSe	Visible	940	*EQE* 2.18×10^5%	-	3
Graphene/GeSe	Visible	3.5×10^5	*Gain* 1×10^7	10	4
Graphene/ReS_2	Visible	7×10^5	*EQE* 1.7×10^8%	30	5
Graphene/MoS_2	Visible	1.2×10^7	*Gain* 1×10^8	2500	6
Graphene/WS_2	Visible	950	-	7850	7

Reference

1. Y. Liu, B. N. Shivananju, Y. Wang, Y. Zhang, W. Yu, S. Xiao, T. Sun, W. Ma, H. Mu, S. Lin, H. Zhang, Y. Lu, C. W. Qiu, S. Li and Q. Bao, *ACS Appl. Mater. Interfaces*, 2017, **9**, 36137–36145.
2. W. Yu, S. Li, Y. Zhang, W. Ma, T. Sun, J. Yuan, K. Fu and Q. Bao, *Small*, 2017, **13**, 1700268.
3. Z. Chen, J. Biscaras and A. Shukla, *Nanoscale*, 2015, **7**, 5981–5986.
4. R. Lu, J. Liu, H. Luo, V. Chikan and J. Z. Wu, *Sci. Rep.*, 2016, **6**, 19161.
5. B. Kang, Y. Kim, W. J. Yoo and C. Lee, *Small*, 2018, **14**, 1802593.
6. W. Zhang, C.-P. Chuu, J.-K. Huang, C.-H. Chen, M.-L. Tsai, Y.-H. Chang, C.-T. Liang, Y.-Z. Chen, Y.-L. Chueh, J.-H. He, M.-Y. Chou and L.-J. Li, *Sci. Rep.*, 2014, **4**, 3826.
7. C. Lan, C. Li, S. Wang, T. He, Z. Zhou, D. Wei, H. Guo, H. Yang and Y. Liu, *J. Mater. Chem. C*, 2017, **5**, 1494–1500.